Visible light promoted gas phase water splitting using porous $WO_3/BiVO_4$ photoanodes

T. Stoll[a*], G. Zafeiropoulos[a*], I. Dogan[a], H. Genuit[a], R. Lavrijsen[b], B. Koopmans[b] and M.N. Tsampas[a,**]

[a] DIFFER-Dutch Institute For Fundamental Energy Research, De Zaale 20, 5612 AJ Eindhoven, the Netherlands

[b] Department of Applied Physics, Eindhoven University of Technology, 5600 MB Eindhoven, the Netherlands

* First and second authors contributed equally and possess the 1st authorship of the article.

**Corresponding author: m.tsampas@differ.nl

Abstract

We recently described the use of Ti(0) microfibers as anodization substrate for the preparation of TiO_2 nanotubes arrays as porous photoanodes. Here, we report the use of these fibres as scaffold to build porous photoanodes based on a $WO_3/BiVO_4$ heterojunction. The obtained photoelectrodes show promising results under visible light irradiation for water oxidation both in a typical liquid-phase photoelectrochemical setup and in an in-house developed gas phase reactor based on a polymeric electrolyte membrane.

Keywords: Photoelectrochemical H_2 production, polymeric electrolyte membrane, gas phase water-splitting, $WO_3/BiVO_4$ photoanode, visible light

1. Introduction

With the rise of energetic and climatic concerns, a large number of research teams around the world are working on the development of devices to produce hydrogen from water and solar energy. In the ideal case, these photoelectrochemical (PEC) devices or cells would make possible, under light irradiation, the dissociation of water into its fundamental components, hydrogen and oxygen. In this context, the use of semiconductors based water-splitting systems is a promising route towards production of "solar hydrogen" at an affordable price [1,2].

The main challenges in the field are the development of efficient photoelectrodes and scalable reactor design [1-3]. This work focuses on the development of a PEC design which resembles polymeric electrolytic membrane (PEM) electrolysers and thus called PEM-PEC [3]. This type of reactor has the advantage of being compact, robust and easily scalable. However it necessitates porous photoelectrode versus the planar design built on conducting glass substrates of conventional PEC studies. Up to now only simple photoanodes based on TiO_2 or WO_3 have been developed for PEM-PEC applications [4-6]. These materials can absorb only a small fraction of the solar terrestrial illumination - as a result their performance is very limited [4-6]. In order to adapt the PEM-PEC concept to the visible part of the solar spectrum, the scope of this article is to investigate the possibility of using the well-known heterojunction $WO_3/BiVO_4$ [2,7].

$BiVO_4$ in its scheelite type monoclinic phase possesses promising properties for applications as photoanode in photoelectrochemical cells. With a ~2.4 eV band gap, it can, in theory, under 1 sun illumination produce photocurrents up to 7 $mA{\cdot}cm^{-2}$ for the water splitting reaction at the thermodynamic potential [1,2]. However, in practice, this material is susceptible to fast hole/electron pair recombination leading to a significant performance drop [7-9]. Some solutions have been tested to overcome this issue: the addition of a doping metal (e.g. W, Mo) [8,9] to diminish the recombination or the association with another semi-conductor through the formation of an heterojunction (i.e. $WO_3/BiVO_4$) to enhance the charge separation [7]. WO_3 is a semiconductor with an indirect band-gap around 2.8 eV that provides light absorption in the near UV and at the beginning of the visible spectrum [1] and has recently been reported to be compatible with titanium microfibers as electric back contact [10]. Due to its good charge carrier properties and to the band alignment with the bands of $BiVO_4$, the electrons from the $BiVO_4$ conduction band can be injected into WO_3, enhancing the charge separation and thus the efficiency [1,2,7].

In this study we built $WO_3/BiVO_4$ heterojunctions, on porous titanium substrates by combining electrochemical anodization of sputtered tungsten layers and $BiVO_4$ formation via SILAR (Successive Ionic Layer Adsorption and Reaction) [11] method, and successfully used them to perform gas phase water-splitting. While most of the common methods (i.e. spin-coating, doctor blade, hydrothermal synthesis) [2] are not usable, the aforementioned preparation techniques suit the nature and the specific porous morphology of the electrode substrate particularly well, while most of the common methods (i.e. spin-coating, doctor blade, hydrothermal synthesis) [2] are not usable.

2. Experimental

W thin films were deposited by DC magnetron sputtering (Kurt J. Lesker) from a 2 in. metallic W target (Kurt J. Lesker) on Ti substrates (Bekaert) of 0.3mm thickness, 80% porosity, 20μm microfibers and 99.9% purity [3]. W-deposition was carried out with base pressure ~10^{-8} mbar, target-substrate distance of 95mm at 25°C, under Ar pressure of 1 Pa, and power of 100 W. The resulting W-film thickness was 200 nm. WO_3 layers were formed through anodization of the 200 nm layer of W(0). To form the oxide a potential of 30 V was applied for 2 min in an ethylene glycol solution containing 0.3 %wt NH_4F and 2 %vol H_2O. Then the electrode was rinsed with water prior to a calcination step (500°C for 1h). One SILAR cycle for the $BiVO_4$ deposition is described as follows: the electrode is dipped for 1 min in a 0.05 M $BiNO_3$ solution, dried for 1 min, rinsed in miliQ-water for 30 s, dried for 30 s, dipped in 0.05 M ammonium metavanadate (NH_4VO_3) (pH=2) solution for 1 min, dried 1 min, rinsed in miliQ water for 30 s and dried 30 s. Once the desired number of cycles is reached the samples are calcined at 550°C for 1h and then etched for 20 min in 1M KOH solution to remove the unwanted vanadium

binary oxide (V_2O_5) [12]. The amount of deposited $BiVO_4$ is therefore controlled by the number of performed cycles.

Surface morphologies of the photoanodes were characterized with a Scanning electron microscope (FEI Quanta 3D FEG instrument) at an acceleration voltage of 30 keV and working distance of 10 mm. The crystal phases were analyzed by X-ray diffraction (Brucker D8 Advance Eco) using a Cu K_α tube. Diffuse reflectance spectra were obtained using a UV-Vis spectrophotometer (PerkinElmer-Lamda 1050) with an integrating sphere attachment (150 mm InGaAs). A Hiden QGA quadrupole mass spectrometer (M/S) operating in selected ion mode with a SEM detector was used for the detection of oxygen and hydrogen in the anodic and cathodic gas streams. Raman spectroscopy measurements were performed with a Renishaw Raman microscope equipped with a 514 nm laser, a grating with 1800 lines/mm, and a CCD detector, and with a measurement step size of 1.7 cm^{-1}. The laser power during measurements is fixed at 0.3 $W.mm^{-2}$.

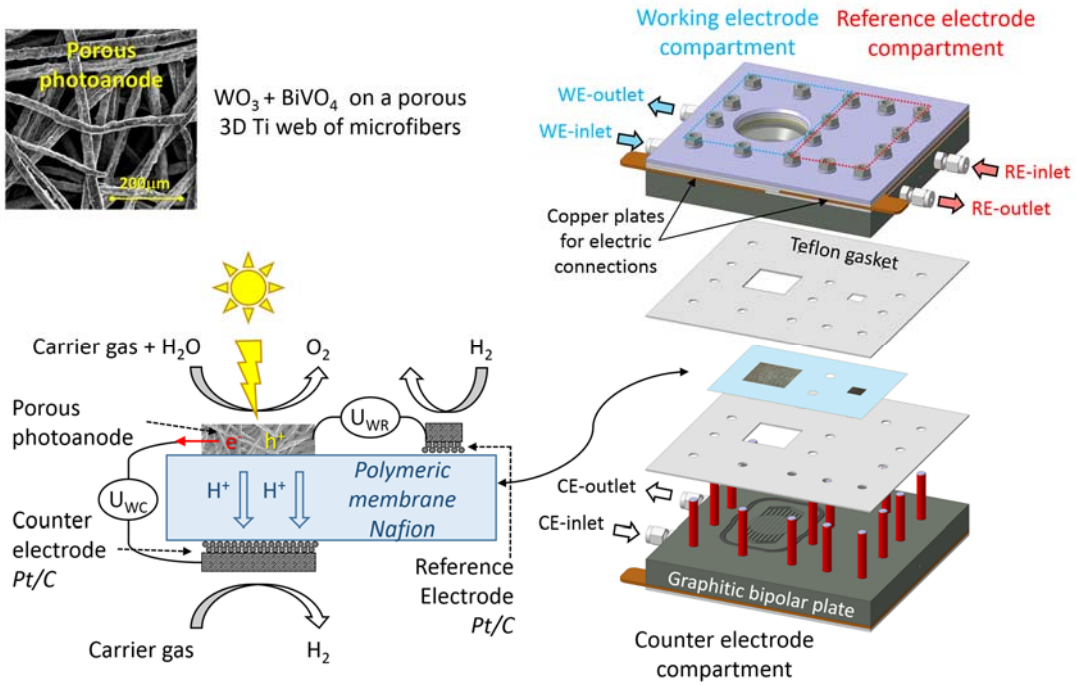

Fig.1 (Left) Configuration and operation of the membrane (photo)electrode assembly. (Right) Novel PEM-PEC reactor design with three compartments for accommodating photoanode, cathode and reference electrodes [3].

The photoelectrodes (geometrical area ca. 1 cm^2) were illuminated using a 150 W Xe lamp (66477-150XF-R1, Newport) with a UV cut-off filter (<395 nm) and an IR removal water filter, where the light intensity was adjusted with a reference cell and meter certified by Newport (91150V) to 100 $mW.cm^{-2}$ on the photoelectrode surface. The lamp in both cases was positioned in the same distance (3 cm) from the photoelectrode surface and the illumination density was measured in both conventional and

PEM-PEC reactors to ensure that the power is the same. The dark current and photo-current of the working electrode versus the external bias voltage were recorded using an Ivium-CompactStat potentiostat, at a 10 $mV.s^{-1}$ scan-rate. Liquid phase photoelectrochemical water-splitting experiments were performed at pH=1 (0.1 M H_2SO_4) in conventional PEC cell while gas phase experiments were carried out in our novel PEM-PEC cell (Fig.1) both are precisely described in a previous paper [3]. Each compartment of the PEM-PEC was fed with gaseous streams, made by bubbling He or air for anodic, He for cathodic and H_2 for reference compartment (at 50 $ml.min^{-1}$) through thermostated gas saturators (at 25°C) containing H_2O, leading to 3.5 vol% H_2O in the feeds.

3. Results and discussion

3.1. Structural analysis: Five samples were characterized: pure Ti/TiO_2 substrate (Ti_{web}), and substrates covered with W(0), WO_3, $BiVO_4$ and $WO_3/BiVO_4$. Fig.2A shows the XRD patterns of the different prepared samples. Typical diffraction peaks from the titanium substrate (black line) are clearly observed for all the samples, along with some smaller signals that can be attributed to a thin over-layer of rutile TiO_2 [3]. In the XRD pattern of the W(0) sputtered sample (blue line) three new signals can be seen at 44, 58 and 74 degrees in good agreement with literature [2,4]. Those peaks are still present after the anodization plus annealing processes (green line) suggesting the formation of a thin WO_3 layer since none of its typical peaks are detected.

Analysis of the $Ti_{web}/BiVO_4$ sample (orange line) shows that in addition to the substrate ones, typical peaks for a monoclinic scheelite structure at angle values of 19, 29, 35, 40, 42, 45, 47, 53, and 58 [2,4]. These signals are still visible on the complete multilayered sample XRD pattern (red line) confirming the success of the $BiVO_4$ deposition process onto the WO_3. Since consecutive annealing steps were carried out for the fabrication of the $WO_3/BiVO_4$, the crystallinity of the WO_3 under-layer has changed compared to the Ti_{web}/WO_3 sample (green line). Thus, additional peaks at 24 and 29 degrees are observed in the spectrum of the $Ti_{web}/BiVO_4$ sample (orange line), which are attributed to WO_3 [4].

As additional characterization we have performed Raman spectroscopy on the prepared photoanodes. This technique allows monitoring the local structure of the material and its bonding states near the surface. Therefore, we expect information mainly from the deposited WO_3 and/or $BiVO_4$ layers. Fig.2B depicts the Raman spectra of WO_3 (green), $BiVO_4$ (orange) and $WO_3/BiVO_4$ (red) deposited on Ti_{web}. For the WO_3 structures, four main peaks are located at 272, 326, 717 and 807 cm^{-1} in good agreement with literature [13]. $BiVO_4$ spectra has six characteristic peaks located at 129, 213, 326, 366, 718 and 827 cm^{-1} [14]. It is clearly seen that the mixed structure $WO_3/BiVO_4$ has features both from WO_3 and $BiVO_4$ structures. The peak located at 815 cm^{-1} is a combination of the stretching mode of WO_3 located at 805 cm^{-1} and the stretching mode of $BiVO_4$ located at 827 cm^{-1}.

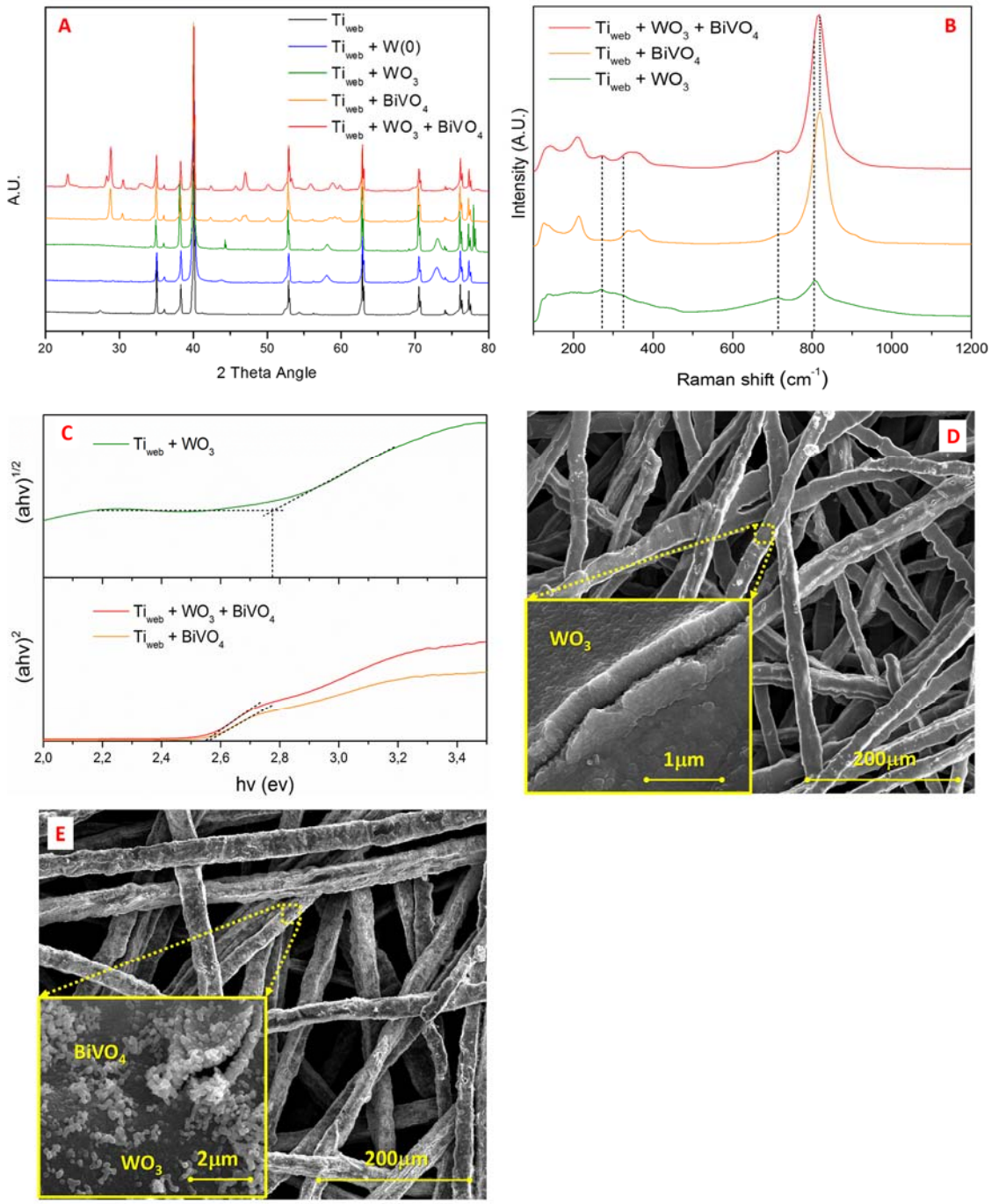

Fig.2 (A) XRD diffraction patterns of the initial Ti_{web} and with different added layers. (B) Raman spectra of Ti_{web} based photoanodes covered by WO_3, $BiVO_4$ and $WO_3/BiVO_4$. (C) Tauc plot of the photoanodes for band gap determination. SEM images of Ti_{web} covered by (D) WO_3 and (D) $WO_3/BiVO_4$. $BiVO_4$ and $WO_3/BiVO_4$ have loading of 40-SILAR-cycles.

The optical band gap of our photoanodes was determined by the following Tauc equation: $(ah\nu)^n=A(h\nu-Eg)$ where A=constant, $h\nu$=light energy, Eg=optical band gap energy, a=measured absorption coefficient, n=0.5 for indirect band gap, and n=2 for direct band gap materials [13]. WO_3

and $BiVO_4$ have an indirect and direct band gap respectively, thus the y axis of the Tauc plot is $(ah\nu)^{1/2}$ for WO_3 and $(ah\nu)^2$ for $BiVO_4$. In the Fig.3B, the extrapolation of the Tauc plot on x intercepts gives the optical band gaps of 2.77, 2.53 and 2.54 eV for Ti_{web} photoanodes covered by WO_3, $BiVO_4$ and WO_3/BiVO4 respectively. These values are in good agreement with literature [15].

The surface morphology of the samples was studied using a scanning electron microscope. Except for some rare cracks, the WO_3 layers appear highly homogeneous (Fig.2D). They show a low roughness, and seem to cover the titanium substrate efficiently. The $BiVO_4$ particles deposited by SILAR method are measured to be around 180 nm and are well distributed on the electrode surface, providing good nanostructuring, even if few agglomerates can be observed in some regions (Fig.2E).

3.2. Photoelectrochemical Characterisation

The synergistic association of WO_3 and $BiVO_4$ has been already well described in the literature [2,7,16]. However, since the type of electrode support and the deposition techniques are different in our case, we initially compared the activities of each photoactive layer separately and prior to the measurement of combined layers.

As shown in Fig.3A, relatively low currents were obtained under irradiation using the two semiconductors individually (0.10 and 0.25 $mA{\cdot}cm^{-2}$ for WO_3 and $BiVO_4$ respectively). The obtained results in the aqueous phase confirm that our fabrication process does form a synergistic WO_3/$BiVO_4$ heterojunction, since the photocurrent in this case can reach up to 2.3 $mA{\cdot}cm^{-2}$.

The crystallinity of the WO_3 photoanode is not the same as WO_3 under layer in the WO_3/$BiVO_4$ photoanodes (Fig.2A) since the fabrication of WO_3/$BiVO_4$ involves consecutive annealing processes. This means that the direct comparison of WO_3 with WO_3/$BiVO_4$ photoanode is not applicable in this case. Nevertheless, as demonstrated in Fig.3A, our main goal to improve the $BiVO_4$ performance building the WO_3/$BiVO_4$ junction has been achieved.

To reach the performance depicted on Fig.3A, we studied the effect of the $BiVO_4$ loading onto the WO_3 layer (Fig.3B). To achieve that, we compared the activity of the WO_3/$BiVO_4$ assemblies after successive steps of 10-SILAR-cycles from 10 until 60-cycles.

All the samples share the same photocurrent onset (about +0.4 V vs RHE) and exhibit a linear current increase through the scanned potentials. At the thermodynamic water oxidation potential the 10-cycles sample give the lowest photocurrent with 0.65 $mA.cm^{-2}$ while the maximum activity, i.e. 1.9 $mA.cm^{-2}$, is reached after 40-cycles. Further SILAR cycles lead to a current drop, thus we consider that the electrode surface starts to get saturated after 40-SILAR-cycles.

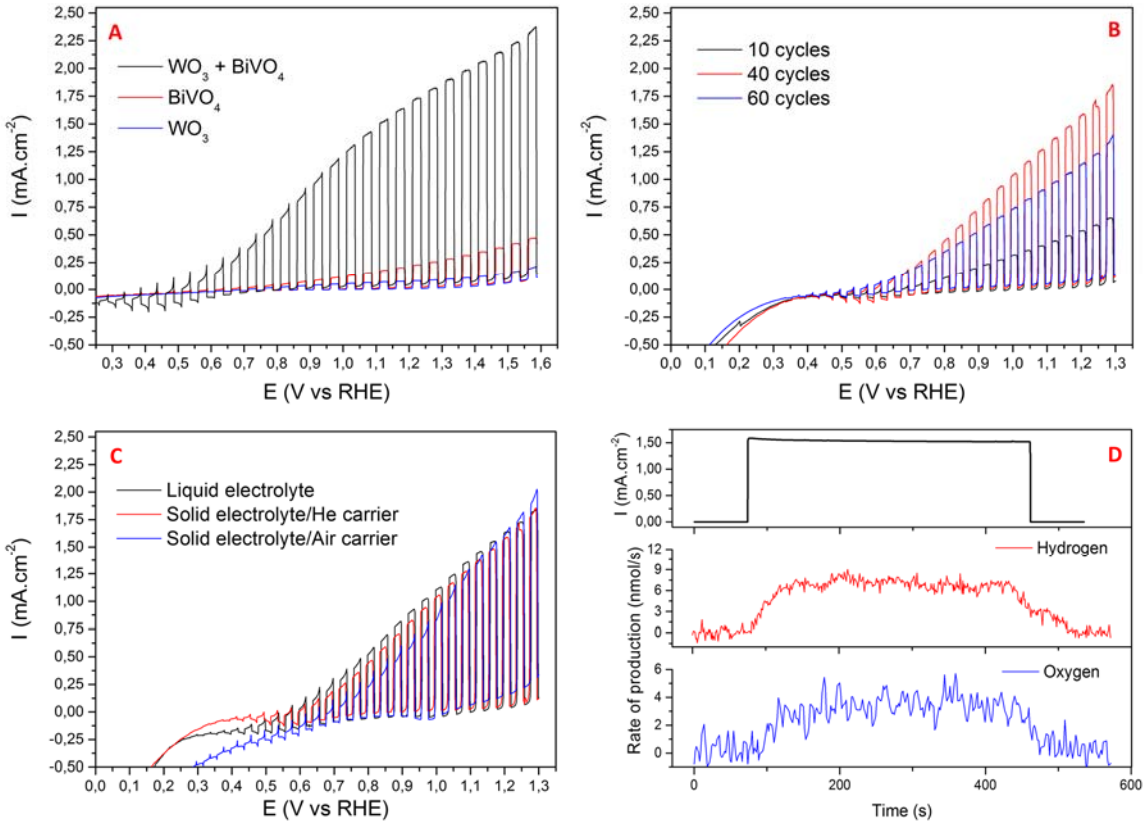

Fig.3 Linear voltammetry sweeps (10 mV/s) of various photoanodes under chopped illumination for water splitting (A) Independent $BiVO_4$ and WO_3 and their coupled conterpart (at 40-SILAR-cycles), (B) Activity of $WO_3/BiVO_4$ photoanodes for different $BiVO_4$ loading (C) 40-SILAR-cycles $WO_3/BiVO_4$ liquid vs gas phase activity (3.5 vol% H_2O in He or Air). (D) Detection of oxygen and hydrogen generation during a step transient illumination experiment for $WO_3/BiVO_4$ (40-SILAR-cycles) at 1.23V vs RHE.

Fig.3C depicts the activity comparison between liquid and solid electrolyte operation (i.e. in PEM-PEC cell). The photoelectrochemical performances are almost identical in terms of photocurrent profile and intensity (1.9 $mA.cm^{-2}$ at the thermodynamic potential) and regarding the photocatalytical current onset (+0.4 V vs RHE). This is several orders of magnitude higher than any other visible light activated solid state electrolyte systems [3-6], confirming the strong potential of our reactor and electrode design.

The possibility of using PEM-PEC cell to capture and use water molecules from the ambient air has been nicely demonstrated by Ronge et al [6]. The potential of this operation mode is based on the fact that solar hydrogen can be produced from a “water-neutral” process. Therefore, we investigated the operation of our PEM-PEC cell using air as carrier gas apart from He (Fig.3C). Molecular oxygen induce current loss through a photoelectron quenching process [3,6] however at high applied potentials the obtained performances were almost identical using the two carriers, showing the great potential of our photoelectrode design for air based PEM-PEC applications.

In order to determine the Faradaic efficiency of our system for splitting reaction, we performed online oxygen and hydrogen detection measurements in anodic and cathodic compartments of the PEM-PEC using a quadrupole M/S for the $WO_3/BiVO_4$ photoanode (of 40-SILAR-cycles). As shown in Fig.3D, the PEM-PEC cell splits water at the rate of 3.4 nmol O_2/s and 7.1 nmol H_2/s (i.e. O_2/H_2 ratio equal to 0.48) at thermodynamic potential. These values correspond to Faradaic efficiency close to ~85%.

The stability of the 40-SILAR-cycles $WO_3/BiVO_4$ photoanode was evaluated at 1.23V vs RHE at conventional operation (i.e. liquid electrolyte). The photocurrent decreases with the time and after 1h of illumination there is a 10% loss of photoactivity. Addition of protective layers (e.g. TiO_2 by atomic layer deposition) and co-catalysts have been planned for improving the stability and activity of our photoanodes.

In general, the obtained results show the good compatibility between the photoanodes and the solid electrolyte PEM-PEC cell design, e.g. the porosity is high enough to maintain the activity while the substrate is exposed to the gas phase reactants.

4. Conclusions

A new preparation method of highly porous $WO_3/BiVO_4$ photoanodes was demonstrated. The photoanodes are efficient under gas phase operation and compatible with our innovative solid electrolyte photoelectrochemical setup. Using our concept, this is the first time that gas phase water splitting exhibits performances similar to those of classical liquid electrolyte photoelectrochemical cells under visible light irradiation and without the use of a co-catalyst.

5. Acknowledgments

This work is part of the programme 'CO_2-neutral fuels', which is financially supported by the Netherlands Organisation for Scientific Research (NWO) and Shell Global Solutions.

6. References

[1] K. Sivula and R. van de Krol, Semiconducting materials for photoelectrochemical energy conversion, Nature Review Materials, 1, 2 (2016) 1510-1527.

[2] R. van de Kroel, M. Gratzel, Photoelectrochemical hydrogen production, New York, Springer 2012

[3] T. Stoll, G. Zafeiropoulos, M.N. Tsampas, Solar fuel production in a novel polymeric electrolyte membrane photoelectrochemical (PEM-PEC) cell with a web of titania nanotube arrays as photoanode and gaseous reactants, International Journal of Hydrogen Energy, 41 (2016) 17807-17817.

[4] J. Georgieva, S. Armyanov, I. Poulios, S. Sotiropoulos, An all-solid photoelectrochemical cell for the photooxidation of organic vapours under ultraviolet and visible light illumination, Electrochemistry Communications, 11 (2009) 1643-1646.

[5] K. Xu, A. Chatzitakis, T. Norby, Solid-state photoelectrochemical cell with TiO2 nanotubes for water splitting, Photochemical and Photobiological Sciences 16 (2017) 10-16.

[6] J. Rongé, S. Deng, S. Pulinthanathu Sree, T. Bosserez, S.W. Verbruggen, N. Kumar Singh, J. Dendooven, M.B.J. Roeffaers, F. Taulelle, M. De Volder, C. Detavernier, J.A. Martens, Air-based photoelectrochemical cell capturing water molecules from ambient air for hydrogen production, RSC Advances, 4 (2014) 29286-29290.

[7] J. Su, L. Guo, N. Bao, C.A. Grimes, Nanostructured WO_3/$BiVO_4$ heterojunction films for efficient photoelectrochemical water splitting, Nano letters, 11 (2011) 1928-1933.

[8] F. F. Abdi, N. Firet, R. van de Krol, Efficient $BiVO_4$ thin film photoanodes modified with Cobalt Phosphate catalyst and W-doping, ChemCatChem, 5 (2013) 490-496.

[9] L. Chen, F.M. Toma, J.K. Cooper, A. Lyon, Y. Lin, I.D. Sharp, J.W. Ager, Mo-doped $BiVO_4$ photoanodes synthesized by reactive sputtering, ChemSusChem, 8 (2015) 1066-1072.

[10] F. Amano, A. Shintani, K. Tsurui, Y.M. Hwang, Fabrication of tungsten trioxide photoanode with titanium microfibers as a three dimensional conductive back contact, Materials Letters, 199 (2017) 68-71.

[11] Y. Li, J. Zhu, H. Zhou, J. Wei, F. Liu, M. Lv, J. Tang, B. Zhang, J. Yao, Z. Huo, L. Hu, S. Dai, $BiVO_4$ semiconductor sensitized solar cells, Science China Chemistry, 58 (2015) 1489-1493.

[12] T. W. Kim, K.S. Choi, Nanoporous $BiVO_4$ photoanodes with dual-layer oxygen evolution catalysts for solar water splitting, Science, 343 (2014) 990-994.

[13] L. Xu, M-L Yin, S. Liu, Agx@WO_3 core-shell nanostructure for LSP enhanced chemical sensors, Scientific reports, 4 (2014) 6745 1-7.

[14] J Yu and A. Kudo, Effects of structural variation on the photocatalytic performance of hydrothermally synthesized $BiVO_4$, Advanced Functional Materials, 16 (2006) 2163–2169.

[15] S.J. Hong, S. Lee, J.S. Jang, J.S. Lee, Heterojunction $BiVO_4$/WO_3 electrodes for enhanced photoactivity of water oxidation, Energy and Environmental Science, 4 (2011) 1781-1787.

[16] L. Xia, J. Bai, J. Li, Q. Zeng, X. Li, B. Zhou, A highly efficient BiVO4/WO3/W heterojunction photoanode for visible-light responsive dual photoelectrode photocatalytic fuel cell, Applied Catalysis B: Environmental, 183 (2016) 224–230.